Machine Learning Driven Synthesis of Carbon Dots with Enhanced Quantum Yields

Yu Han,[†,¶] Bijun Tang,[§,¶] Liang Wang,[*,†] Hong Bao,[†] Yuhao Lu,[#] Cuntai Guan,[#] Liang Zhang,[†] Mengying Le,[†] Zheng Liu,[*,§] and Minghong Wu[*,‡]

[†]Institute of Nanochemistry and Nanobiology, School of Environmental and Chemical Engineering, Shanghai University, 99 Shangda Road, BaoShan District, Shanghai 200444, P.R. China

[§]School of Materials Science and Engineering, Nanyang Technological University, 50 Nanyang Avenue, Singapore 639798, Singapore

[#]School of Computer Science and Engineering, Nanyang Technological University, 50 Nanyang Avenue, Singapore 639798, Singapore

[‡]Shanghai Applied Radiation Institute, Shanghai University, 333 Nanchen Road, BaoShan District, Shanghai 200444, P.R. China

[¶]These authors contributed equally to this work.

To whom correspondence should be addressed: Tel: +86-21-66135276.

*E-mail: wangl@shu.edu.cn (L. Wang); z.liu@ntu.edu (Z. Liu); mhwu@shu.edu.cn (M. Wu).

ABSTRACT: Knowing the correlation of reaction parameters in the preparing process of carbon dots (CDs) is essential for optimizing the synthesis strategy, exploring exotic properties, and exploiting potential applications. However, the integrated screening experimental data on the synthesis of CDs are huge and noisy. Machine learning (ML) has recently been successfully used

for the screening of high-performance materials. Here, we demonstrate how ML-based techniques can offer insight into the successful prediction, optimization and acceleration of CDs' synthesis process. A regression ML model on hydrothermal-synthesized CDs is established capable of revealing the relationship between various synthesis parameters and experimental outcome, as well as enhancing the process-related properties such as the fluorescent quantum yield (QY). CDs exhibiting a strong green emission with QY up to 39.3% are obtained through the combined ML guidance and experimental verification. The mass of precursors and the volume of alkaline catalysts are identified as the most important features in the synthesis of high-QY CDs by the trained ML model. The CDs are applied as an ultra-sensitive fluorescence probe for monitoring Fe^{3+} ion because of their superior optical behaviors. The probe exhibits the linear response to Fe^{3+} ion with a wide concentration range (0−150 μM), and its detection limit is 0.039 μM. Our findings demonstrate the great capability of ML to guide the synthesis of high-quality CDs, accelerating the development of intelligent material.

KEYWORDS: *machine learning, carbon dots, process-related properties, quantum yield, sensing*

Fluorescence nanosensors display various superiorities surpass conventional electrochemical methods, including high sensitivity and selectivity naked-eye detection.[1] Compared with the conventional fluorescent nanosensors (*e.g.*, heavy metal-containing quantum dots and organic fluorophores), carbon dots (CDs) are particularly well suited for the study of rapid-responsive sensing in terms of their rapid response time and reversible cycle.[2-4] Particularly, CDs simultaneously exhibit several vital merits for optical sensing such as ease of functionalization,[5] broad-band optical absorption,[6] tunable emission,[7] excellent photostability,[8] and low toxicity.[9] The current primary approach of interest to fabricate CDs is hydrothermal or solvothermal "bottom-

up" preparation method.[10-12] To reveal superior sensing characteristics, research has shown one viable method for identifying high-quality CDs by their fluorescent quantum yield (QYs). The success of high-QYs CDs depends on the tuning of many parameters, such as reaction temperature, the mass of precursor, ramp rate, and reaction time. Nevertheless, current CDs reported in the literature were often optimized preparation by regulate a reaction parameter and fix other reaction factors, as measured by their QYs, and always ignored the correlation of reaction parameters in the synthesis process of CDs, which must be efficiently analyzed. They often lack an effective method to analyze complex relationships. Therefore, understanding the critical factors of the production process is a central problem to synthesize high-QYs CDs, and there is the need for directed evolution to realize intrinsic relation obtained by some transformative ways.

Machine learning (ML), a type of artificial intelligence, has received wide-ranging attention as a robust and versatile tool due to its excellent performance in dealing with a huge amount of data efficiently in various fields.[13,14] ML-driven approaches have been applied in numerous research domains successfully, such as recognition,[15] physics,[16] chemistry,[17-20] and biology,[21-24] as well as materials science. More importantly, ML has demonstrated exceptional capability to accelerate the development of novel materials, through effectively learning from the past and even failed data.[25-30] Although ML has been primarily employed for the discovery of innovative materials, high prediction accuracy to their properties and strong adaptability, ML-assisted synthesis remains less investigated, mainly due to the highly complicated synthesis process and small dataset. Consequently, the feasibility and potential of introducing ML into the high-QYs CDs synthesis to expedite the exploration period and reduce the cost are worthy of being investigated.

Herein, an ML-assisted synthesis way is reported for the manufacture of highly fluorescent CDs by the hydrothermal route. We demonstrate here using ML in the synthesis process can enhance

the optical properties of CDs significantly, where the CDs can exhibit strong green emission with its QYs of up to 39.3%. Furthermore, the correlation of reaction parameters of CDs during the produced process was analyzed and identified. Furthermore, as a proof-of-concept demonstration, the optimized CDs are utilized for the supersensitive, rapid, and specific detection of iron ion (Fe^{3+}) in the concentration range of 0−150 μM, and the detection limit was achieved to 0.039 μM. Overall, the ML-assisted synthesis strategy plays a vital role in novel materials design and rapid-synthesis in the future.

RESULTS AND DISCUSSION

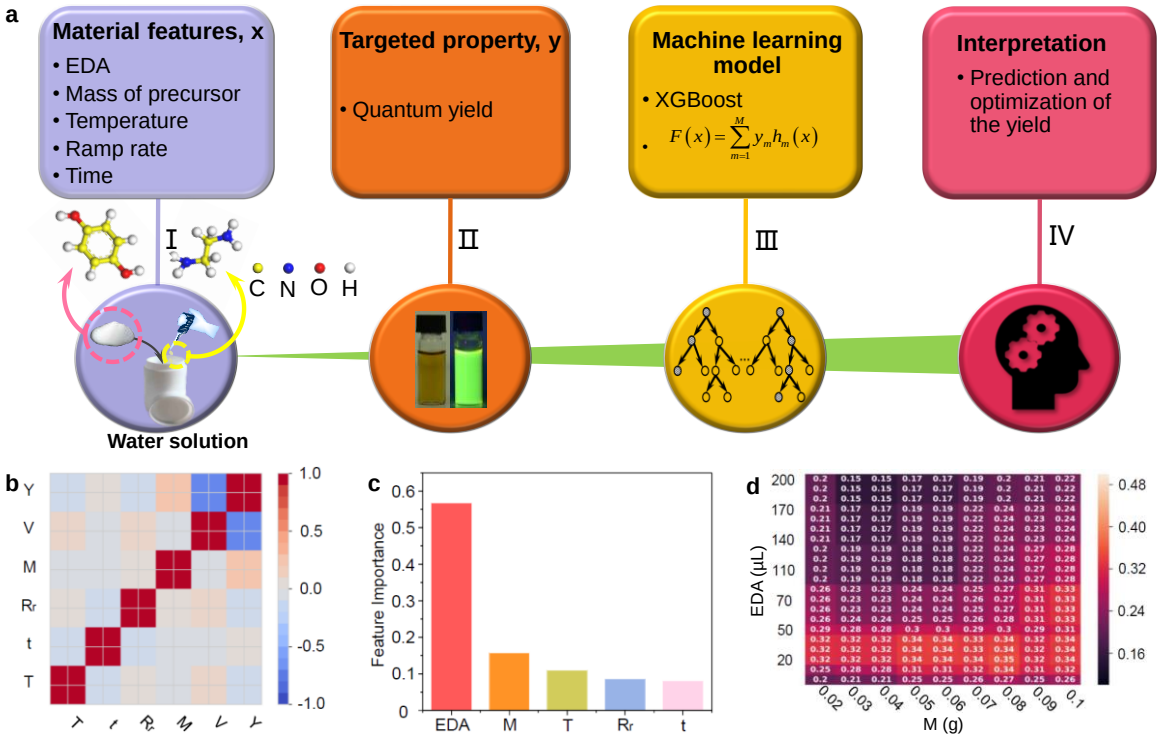

Figure 1. Application of ML for guided synthesis of CDs. (a) Design framework for the guided synthesis of CDs with a large QY based on ML and hydrothermal experiments. (b) The heat map of the Pearson's correlation coefficient matrix among the selected features of hydrothermal-grown CDs. (c) Feature importance retrieved from XGBoost-R that learns

from the full dataset. The most important features are EDA and M. (d) Predictions from the trained model, which is represented by the matrix formed by the two most important features.

The experimental setup for the synthesis of CDs is shown in Figure 1a-I, and the detailed synthesis process is provided in the Experimental section. Empirically, five experimental parameters were identified as significant input features: volume of EDA (μL), mass of precursor (g), reaction temperature (°C), ramp rate (°C/min) and reaction time (h). 391 experiments were carried out in the laboratory with different combinations of growth parameters, and respective QY ranging from 0 to 1 were recorded. Feature correlations between pairs of features were calculated and presented in Figure 1b, with low linear correlations verifying the effectiveness of feature selection. To best infer QY from the feature, several regression models were evaluated with nested cross validation method as reported in our previous work,[31] including XGBoost regressor (XGBoost-R), multilayer perceptron regressor (MLP-R), support vector machine regressor (SVM-R), and Gaussian process regressor (GP-R). Three commonly used performance metrics are adopted to evaluate ML models: coefficient of determination (R^2), mean squared error (MSE) and Pearson's correlation coefficient (r). Model evaluation results are summarized and compared in the boxplot (Figure S1). As indicated, XGBoost-R outperforms all the other three models and is selected as the best model for this study.

To quantitively understand the system of hydrothermal-grown CDs from the perspective of data, feature importance was extracted from the trained XGBoost-R model, with the result shown in Figure 1c. Features with higher importance have stronger impact on the experimental outcome, *i.e.* the value of QY. As indicated, the volume of EDA plays the most important role in determining the QY of formed CDs, followed by mass of precursor and reaction temperature. This result is

very much in line with our expectation. From the experimental aspect to interpret, the EDA is a common addition agent during the preparation of the CDs.[32-35] In this work, it not only acts as an alkaline catalyst, but also acts as a reactant, which can improve the reaction process, provide the N-doping, reduce the degree of defects in the synthesized CDs, and eventually contribute to achieving high-QYs CDs.

Since the QY of the interested CDs system cannot be further improved with the conventional trial-and-error exploration, optimization of the synthesis condition has thus been carried out as per our previous study. Based on the input ranges of each feature for optimization (Table S1), respective QY of the resulted 702,702 combinations have been predicted. To better interpret the information embedded in the as-predicted combinations, the predicted results are represented by a matrix formed by the two most important features, as shown in Figure 1d. The brighter the area, the higher yield might be produced when the two features are within the corresponding ranges. The optimal ranges of the synthesis parameters can, therefore, be easily identified. Specifically, in this system, when the amount of EDA added is between 10-50 μL, regardless of the amount of precursor added, the produced CDs can obtain high QY. It may thus be concluded that the EDA added within this range can promote the synthesis reaction. When the amount of EDA is increased to 60-90 μL, CDs can achieve high QY only when a large number of precursors is added. Moreover, when the amount of EDA added exceeds 100 μL, all the synthesized CDs show a relatively low QY. This is consistent with the rule that excessive addition of EDA changes from promoting the reaction to passivating the surface of the CDs and inhibiting the reaction. Twenty combinations with the highest predicted QY were chosen for experimental verification (Table S2), and high QY of 39.3% was achieved, indicating the feasibility and effectiveness of ML-guided CDs synthesis. Moreover, considering the huge complexity of the XGBoost model, decision tree regressor has

been applied on top of the trained XGBoost-R to generate a human-interpretable decision tree for further analysis. Details are provided in Figure S2. The oval and rectangle represent decision node and reaction-outcome bin, respectively. The value of the bins is generated by the decision tree regressor as a reference, where the higher the value, the larger QY might be produced.

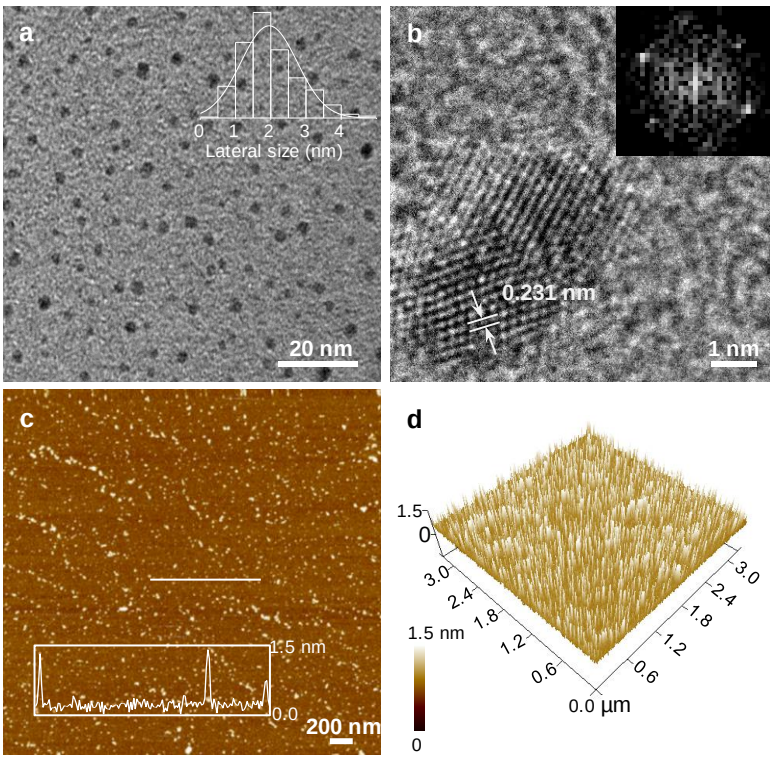

Figure 2. Geometrical characterization of the CDs. (a) TEM image and size distribution of CDs. (b) The high-resolution TEM image of CDs (inset: fast Fourier transform patterns). (c) AFM image and thickness distribution of CDs at the white line. (d) 3D AFM image of CDs.

Transmission electron microscopy (TEM) and atomic force microscopy (AFM) were employed to investigate the morphology and thickness of optimized CDs. The well-dispersion of CDs is observed from the TEM images in Figure 2a and has an average size of 2 nm. A crystalline structure of the CDs with a lattice distance of 0.231 nm are shown in the high-resolution TEM image (Figure 2b), corresponding well to the (002) lattice plane of graphite.[32] It is also confirmed from the X-ray diffraction (XRD) spectrum in Figure 3a that there is a broad peak at $2\theta = 25.6°$.[5]

Regardless of their interplanar distance, the hexagonal carbon network from the corresponding fast Fourier transform (FFT) image can also illustrate that the CDs have the crystalline structure.[36] The CDs has a height distribution peaked at 1.5 nm in Figure 2c, demonstrating there are elliptical structure corresponding to the definition of CDs. Figure 2d is a three-dimensional (3D) plot of Figure 2c. It is worthy to note that the thicknesses of majority CDs are practically 1.4 nm, indicating that the CDs produced by the ML-assisted synthesis approach can obtain the resemble morphology and further display excellent performance.

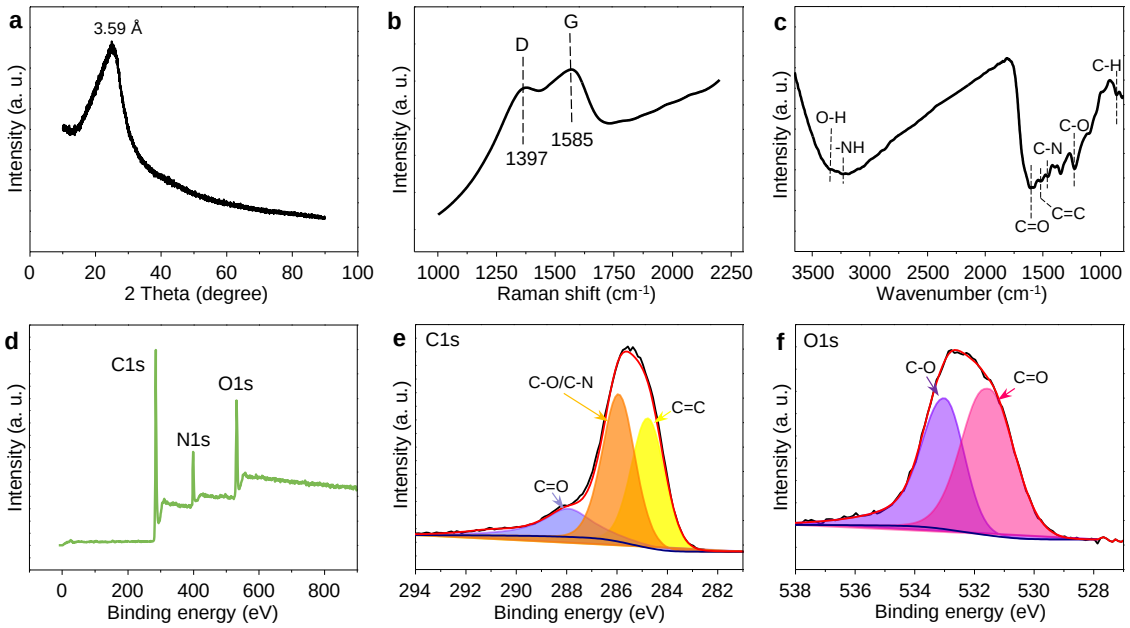

Figure 3. (a) XRD pattern of CDs. (b) Raman spectrum of CDs. (c) FT-IR spectrum of CDs. (d) XPS survey spectrum of CDs. (e) XPS C1s spectrum of CDs. (f) XPS O1s spectrum of CDs.

Further analyses were carried out to verify the structure and surface functional groups of CDs. High-degree graphitization is examined by the Raman spectrum (Figure 3b), where the signal of the ordered G band located at 1585 cm^{-1} is larger than that of the disordered D band at 1397 cm^{-1}. Meanwhile, the G to D intensity ratio for the CDs were found to be 1.13, which is illustrated by

the interlayer spacing value (3.59 Å) of the CDs (Figure 3a).[37] To verify that the existence of various functional groups in CDs, the Fourier-transform infrared (FT-IR) spectroscopy is measured (Figure 3c). The −NH and N−C stretching (about 3234 and 1457 cm^{-1}), indicating there are a huge number of NH_2 groups on the surface of CDs.[38-40] Meanwhile, the C=C aromatic ring stretch was located at 1510 cm^{-1}. On the other hand, three oxide-related peaks, O−H, C=O and C−O stretching were noticed at 3480, 1580 and 1240 cm^{-1} due to abundant hydroxyl groups in the precursor.[41] X-ray photoelectron spectroscopy (XPS) was further fulfilled to confirm the functional groups in CDs, whose results are presented in Figure 3d-3f and Figure S3. XPS survey spectrum analysis reveals that there are mainly three kinds of elements (C, O, and N) that make up CDs, with atomic ratios of 71.08%, 16.54%, and 12.38%, respectively (Table S3). The high-resolution C1s spectrum of CDs was deconvoluted to three peaks: a dominant C=C graphitic carbon bond (284.8 eV), a C−O/C−N bond (286 eV), and a C=O carboxyl carbon bond (288 eV).[42-44] N1s peaks at 399.7 eV indicate the existence of N−C bonds, confirming that the N atoms successfully doped in the basal plane network structure of the CDs. O1s separated peaks at 531.5 and 533 eV indicate that oxygen functionalization in CDs has two modality oxyhydrogen functional groups with C=O and C−O, respectively, which is an agreement with the conclusions of the FT-IR spectrum. The high QY of CDs may be originated from the N-doping of CDs. N-doping can reduce the non-radiative sites of CDs, which can be beneficial to the formation of C=O bonds. The existence of C=O bonds of CDs lead to extensive radiation recombination and then increase their QY.[45] From the above morphology and structure analysis, we discover that the CDs with high QY seems to be a single-layer and high-crystallinity graphene-like material of CDs. So high-crystallinity and few-thickness of CDs can improve the fluorescence performance. In short,

CDs have high-level graphitized structure and the successful N, O co-dopant in CDs, enhancing its water solubility and ion detection selectivity in practical application.

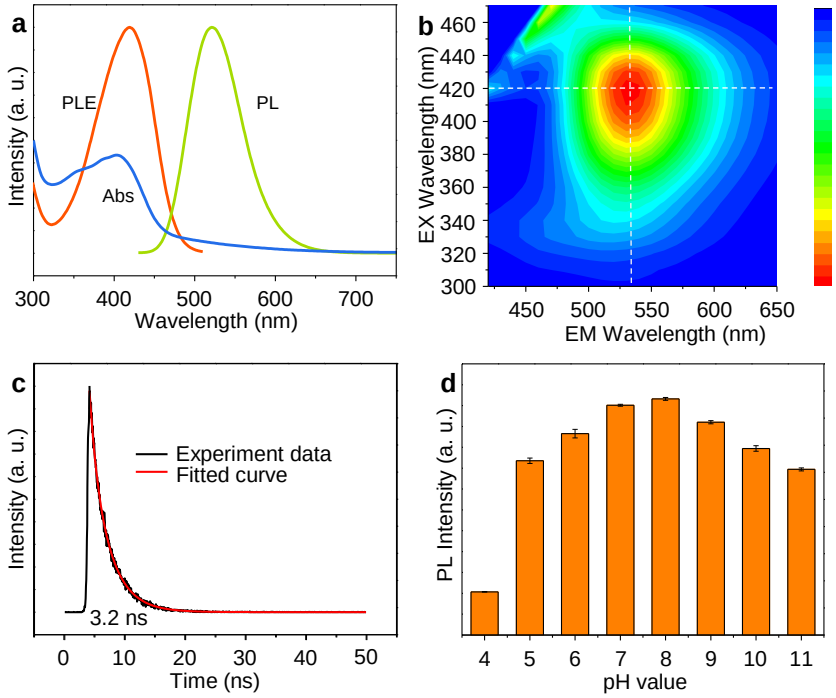

Figure 4. Optical characterizations of CDs. (a) UV−Vis absorption, PL, and PLE spectra of CDs. (b) The 3D fluorescence plots of CDs. (c) Time-resolved PL spectrum of CDs. (d) Dependence of PL intensity of CDs at different pH values (4–10) (n = 3 for each group).

Furthermore, we investigated the optical performance of the selected CDs. The UV–vis absorption spectrum of the CDs in Figure 4a is observed a typical absorption peak at 420 nm, which is consistent with the optimum photoluminescence (PL) excitation wavelength in PL excitation (PLE) and emission spectra. Comparison with the conclusions from other published work, the maximum green emission wavelength and PLE wavelength are located at 520 nm and 420 nm, respectively. The full width at half maximum of the PL spectrum is narrow to 95 nm due to the high-degree graphitization and crystalline. It is worth noting that they displayed excitation independent characteristic with regular intervals on the excitation wavelength (Figure 4b and

Figure S4), suggesting that CDs could serve as a stable optical fluorescent probe avoiding the experimental error caused by the shift of PL excitation wavelength.[46,47] Owing to its excitation independent property, the lifetime decay curve of the CDs displays a single exponential decay characteristic with a 3.2 ns lifetime (Figure 4c). To investigate the solution stability of CDs at different times, we choose water, methanol, ethanol, isopropanol as solutions. As shown in Figure S5, the fluorescence intensity of CDs in ethanol solution remained unchanged within 24 h, and above 93% in the long-term stability test. Besides, the CDs exhibits similar stability phenomena in the other three solutions. the fluorescence intensity of CDs in these solutions remained slightly decreased within 24 h, and reduced by ~80% in the long-term measurement, showing that the CDs has comparable stability in different solutions. Furthermore, the PL stability of CDs under different pH conditions was also investigated (Figure 4d and Figure S6). The fluorescence intensity of the CDs gradually decreases under strongly acidic or alkaline conditions. On the contrary, the strength of PL holds the stability in the mid environment (pH = 4−9), which is suitable for monitoring the metal ion in solution as an efficient probe.

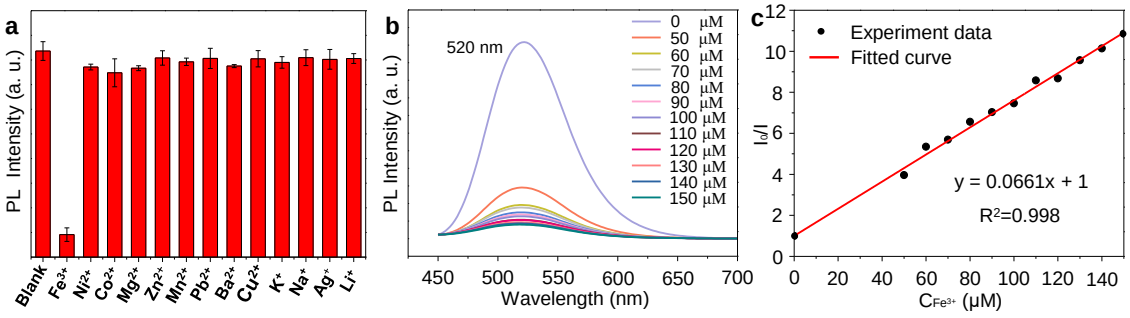

Figure 5. Metal ion sensing performance of CDs. (a) Selectivity and sensitivity of CDs for different metal ions (n = 3 for each group). (b) PL spectra of CDs in the presence of different Fe^{3+} concentrations. (c) The dependence of the I_0/I value on Fe^{3+} concentrations.

Recently, ion detection relied on CDs fluorescence has been rapidly developed.[48-50] Among the 13 selected ions, only Fe^{3+} ion has shown an obvious fluorescence quenching effect on CDs in Figure 5a, exhibiting the high sensitivity to Fe^{3+} ion. The possible quench mechanism is that Fe^{3+} ion has a strong binding affinity with N, O functional groups in CDs, but also electron transfer with the optically active sites of CDs.[38] Once adding Fe^{3+} ion solution into the CDs solution, the fluorescence quenching phenomenon of CDs appears. To further study the interaction between Fe^{3+} ion and CDs, the fluorescence changes of CDs in the existence of Fe^{3+} ion with different concentrations were surveyed. With the gradual increase of Fe^{3+} ion concentration (0−150 μM), the fluorescence intensity is decreasing (Figure 5b).[38] In addition, there is a good linear relationship between the I_0/I value and the Fe^{3+} concentrations (0−150 μM) with a high correlation coefficient of 0.998 in Figure 5c.[51] Furthermore, the limit of detection (LOD) for Fe^{3+} ion was calculated to be 0.039 μM, exceeding that of the majority published CDs. The Stern–Volmer constant (Ksv) is 66.1 M^{-1}.[52] The reversibility of CDs in metal ion sensing is a crucial factor in practical application. When Fe^{3+} ion and ascorbic acid were alternately added to the CDs solution, the fluorescence intensity could be switched for 2 cycles without obvious lost (Figure S7), which displayed that the CDs-based metal ion fluorescent probe could be regenerated. Eventually, the prepared CDs provide a highly sensitive and convenient platform for reversible detecting Fe^{3+} ion.

CONCLUSIONS

In summary, we introduced an ML strategy to successfully predict, optimize and accelerate the CDs' synthesis process, elucidate the correlation of reaction factors of CDs and further bridge the gap between theory and experimental realization. In light of the data from experiments and ML analysis, the QYs of bright green fluorescent CDs can achieve up to 39.3%. The trained ML model further revealed that the excellent optical properties are strongly associated with the mass of

precursor and volume of the alkaline catalyst, which is in good agreement with experimental findings. More importantly, we have applied the high-quality CDs to sense Fe^{3+} ion in solution. The probe displayed a wide linear response concentration range (0−150 μM) to Fe^{3+} ion with a detection limit of 0.039 μM, revealing its high-sensitive and high-selective performances. It is worth mentioning that the focus of this work is to use ML to improve QYs by optimizing a few hydrothermal synthesis parameters. Even though satisfactory progress has been made, there is still a plenty of room for the improvement of QYs, which is now limited by the few features involved in current work. Apart from the synthesis parameters, chemistry-related features such as types of precursors, types of catalysts, types of solvent and *etc.*, can also affect the QYs significantly. The establishment of a more comprehensive model involving both synthesis process-related and chemistry-related features will be a promising prospect for improvement, which will be carried out in our future work. Nevertheless, the approach presented in this work is a steppingstone toward developing artificial intelligence approaches to analyze and optimize the material preparation method. We envision that a reliably artificial general intelligence system for nanomaterials science will be easily generalized to many other candidates' systems in the future.

EXPERIMENTAL SECTION

Materials. All chemicals were obtained from the commercial suppliers without further purification. The p-dihydroxybenzene (p-Db), and ethylenediamine (EDA) were purchased from Sinopharm Chemical Reagent Co., Ltd (China).

Preparation of the CDs. Briefly, p-Db (0.02-0.1 g) and EDA (0-200 μL) were dissolved in 10 mL of DI water and ultra-sounded for 10 min. Subsequently, the mixture was transferred into a poly(tetrafluoroethylene) (Teflon)-lined autoclave in an oven with a ramp rate of 5-30°C/min at 100-220°C for 2-12 h. After cooling down to room temperature, the CDs solution was obtained

and thereafter filtered using a 0.22 μm microporous membrane. Then the CDs solution was dialyzed against a dialysis bag (MW: 3000 Da) for several days. The dialyzed solution was subjected to further vacuum drying to obtain CD powders.

Characterization. The fluorescence spectra were performed on a Hitachi 7000 fluorescence spectrophotometer. The time-resolved PL spectrum was analyzed on an Edinburgh FS5 spectrofluorometer. Additionally, the absorption spectrum was conducted on a Hitachi 3100 spectrophotometer. AFM image was obtained using the Bruker 8 AFM system. TEM image was measured by the JEOL JEM-2010f electron microscope operating at 200 kV. XPS data were achieved with an AMICUS electron spectrometer from SHIMADZU using 300 W Alkα radiation. Raman spectroscopy was carried out on a Renishaw in plus laser Raman spectrometer with 633 nm. XRD pattern was recorded on a Rigaku D/max-2500 with Cu Ka radiation. FT-IR spectrum was recorded using the Bio-Rad FTS165 FT-IR spectrometer. Zeta potentials of CDs were measured on a ZS90 Malvern Zetasizer Nano. The QY measurement referred to our previous work.[37]

Detection of Fe^{3+}. The standard solutions of 13 metal ions (Ni^{2+}, Co^{2+}, Fe^{3+}, Mg^{2+}, Zn^{2+}, Mn^{2+}, Pb^{2+}, Ba^{2+}, Cu^{2+}, K^{+}, Na^{+}, Ag^{+} and Li^{+}, the concentration of the selected metal ion is 1 mM) were prepared to detect the interaction between metal ions with the fluorescence of CDs. To quantitatively measure the effect of Fe^{3+} concentration on CDs solution, a series of $FeCl_3$ solutions with the different concentrations of Fe^{3+} ion (0−150 μM) were performed. In opposite, the concentration of CDs was consistent. Their fluorescence intensity was measured using a fluorescence spectrophotometer after mixing for 10 minutes. We used ascorbic acid to recover the fluorescence of CDs, which was quenched by Fe^{3+} ion.

ASSOCIATED CONTENT

Supporting Information

The Supporting Information is available free of charge on the ACS Publications website.

Boxplots of the four candidate models' coefficient, XGBoost-derived decision tree, XPS N1s spectrum of CDs, PL spectra of CDs excited by different excitation wavelengths, the stability of CDs *vs* times and at different solutions, ABS, PL spectra and Zeta potential of CDs at different pH values, reversible cycle of CDs, input range of parameters in the hydrothermal system, combinations with the highest probability, and the elements ratio of CDs in XPS survey spectrum.

The authors declare no competing financial interest.

AUTHOR INFORMATION

Corresponding Author

*E-mail: wangl@shu.edu.cn (L. Wang).

*E-mail: z.liu@ntu.edu (Z. Liu).

*E-mail: mhwu@shu.edu.cn (M. Wu).

ORCID

Liang Wang: 0000-0002-3771-4627

Zheng Liu: 0000-0002-8825-7198

Minghong Wu: 0000-0002-9776-671X

Author Contributions

¶Y. Han and B. Tang contributed equally to this work.

ACKNOWLEDGMENTS

Yu Han checked the raw data and ensured their authenticity. The project was funded by National Natural Science Foundation of China (Nos. 21671129, 21901154, 21671131), the Shanghai Sailing Program (No. 16YF1404400), the Program for Changjiang Scholars and Innovative Research Team in University (No. IRT17R71). We thank the Laboratory for Microstructures of Shanghai University. Z. Liu acknowledges the financial support from Singapore Ministry of Education AcRF Tier 1 (RG161/19).

REFERENCES

(1) Sun, H.; Wu, L.; Wei, W.; Qu, X. Recent Advances in Graphene Quantum Dots for Sensing. *Mater. Today* **2013**, *16*, 433-442.

(2) Kalytchuk, S.; Polakova, K.; Wang, Y.; Froning, J. P.; Cepe, K.; Rogach, A. L.; Zboril, R. Carbon Dot Nanothermometry: Intracellular Photoluminescence Lifetime Thermal Sensing. *ACS Nano* **2017**, *11*, 1432-1442.

(3) Kong, B.; Zhu, A.; Ding, C.; Zhao, X.; Li, B.; Tian, Y. Carbon Dot-Based Inorganic-Organic Nanosystem for Two-Photon Imaging and Biosensing of pH Variation in Living Cells and Tissues. *Adv. Mater.* **2012**, *24*, 5844-5848.

(4) Chen, T.-H.; Tseng, W.-L. Self-Assembly of Monodisperse Carbon Dots into High-Brightness Nanoaggregates for Cellular Uptake Imaging and Iron(III) Sensing. *Anal. Chem.* **2017**, *89*, 11348-11356.

(5) Miao, X.; Qu, D.; Yang, D. X.; Nie, B.; Zhao, Y. K.; Fan, H. Y.; Sun, Z. C. Synthesis of Carbon Dots with Multiple Color Emission by Controlled Graphitization and Surface Functionalization. *Adv. Mate*r. **2018**, *30*, 1704740-170474.

(6) Ding, H.; Yu, S. B.; Wei, J. S.; Xiong, H. M. Full-Color Light-Emitting Carbon Dots with a Surface-State-Controlled Luminescence Mechanism. *ACS Nano* **2016**, *10*, 484-491.

(7) Pan, L. L.; Sun, S.; Zhang, A. D.; Jiang, K.; Zhang, L.; Dong, C. Q.; Huang, Q.; Wu, A. G.; Lin, H. W. Truly Fluorescent Excitation-Dependent Carbon Dots and Their Applications in Multicolor Cellular Imaging and Multidimensional Sensing. *Adv. Mater.* **2015**, *27*, 7782-7787.

(8) Benetti, D.; Jokar, E.; Yu, C.-H.; Fathi, A.; Zhao, H.; Vomiero, A.; Diau, E. W.-G.; Rosei, F. Hole-Extraction and Photostability Enhancement in Highly Efficient Inverted Perovskite Solar Cells Through Carbon Dot-Based Hybrid Material. *Nano Energy* **2019**, *62*, 781-790.

(9) Peng, J.; Gao, W.; Gupta, B. K.; Liu, Z.; Romero-Aburto, R.; Ge, L.; Song, L.; Alemany, L. B.; Zhan, X.; Gao, G.; Vithayathil, S. A.; Kaipparettu, B. A.; Marti, A. A.; Hayashi, T.; Zhu, J.-J.; Ajayan, P. M. Graphene Quantum Dots Derived from Carbon Fibers. *Nano Lett.* **2012**, *12*, 844-849.

(10) Hola, K.; Sudolska, M.; Kalytchuk, S.; Nachtigallova, D.; Rogach, A. L.; Otyepka, M.; Zboril, R. Graphitic Nitrogen Triggers Red Fluorescence in Carbon Dots. *ACS Nano* **2017**, *11*, 12402-12410.

(11) Yang, S.; Li, W.; Ye, C.; Wang, G.; Tian, H.; Zhu, C.; He, P.; Ding, G.; Xie, X.; Liu, Y.; Lifshitz, Y.; Lee, S.-T.; Kang, Z.; Jiang, M. C_3N-A 2D Crystalline, Hole-Free, Tunable-Narrow-Bandgap Semiconductor with Ferromagnetic Properties. *Adv. Mater*. **2017**, *29*, 1605625.

(12) Jiang, K.; Sun, S.; Zhang, L.; Lu, Y.; Wu, A. G.; Cai, C. Z.; Lin, H. W. Red, Green, and Blue Luminescence by Carbon Dots: Full-Color Emission Tuning and Multicolor Cellular Imaging. *Angew. Chem. Int. Ed.* **2015**, *54*, 5360-5363.

(13) Hoffmann, J.; Bar-Sinai, Y.; Lee, L. M.; Andrejevic, J.; Mishra, S.; Rubinstein, S. M.; Rycroft, C. H. Machine Learning in a Data-Limited Regime: Augmenting Experiments with Synthetic Data Uncovers Order in Crumpled Sheets. *Sci. Adv*. **2019**, *5*, eaau6792.

(14) Coley, C. W.; Green, W. H.; Jensen, K. F. Machine Learning in Computer-Aided Synthesis Planning. *Acc. Chem. Res.* **2018**, *51*, 1281-1289.

(15) Li, L.; Ruan, H.; Liu, C.; Li, Y.; Shuang, Y.; Alu, A.; Qiu, C. W.; Cui, T. J. Machine-Learning Reprogrammable Metasurface Imager. *Nat. Commun*. **2019**, *10*, 1082.

(16) Durand, A.; Wiesner, T.; Gardner, M. A.; Robitaille, L. E.; Bilodeau, A.; Gagne, C.; De Koninck, P.; Lavoie-Cardinal, F. A Machine Learning Approach for Online Automated Optimization of Super-Resolution Optical Microscopy. *Nat. Commun*. **2018**, *9*, 5247.

(17) Bonk, B. M.; Weis, J. W.; Tidor, B. Machine Learning Identifies Chemical Characteristics That Promote Enzyme Catalysis. *J. Am. Chem. Soc.* **2019**, *141*, 4108-4118.

(18) Granda, J. M.; Donina, L.; Dragone, V.; Long, D.-L.; Cronin, L. Controlling an Organic Synthesis Robot with Machine Learning to Search for New Reactivity. *Nature* **2018**, *559*, 377-381.

(19) Maryasin, B.; Marquetand, P.; Maulide, N. Machine Learning for Organic Synthesis: Are Robots Replacing Chemists. *Angew. Chem. Int. Ed.* **2018**, *57*, 6978-6980.

(20) Sun, W. B.; Zheng, Y. J.; Yang, K.; Zhang, Q.; Shah, A. A.; Wu, Z.; Sun, Y. Y.; Feng, L.; Chen, D. Y.; Xiao, Z. Y.; Lu, S. R.; Li, Y.; Sun, K. Machine Learning-Assisted Molecular Design and Efficiency Prediction for High-Performance Organic Photovoltaic Materials. *Sci. Adv.* **2019**, *5*, eaay4275.

(21) Heckmann, D.; Lloyd, C. J.; Mih, N.; Ha, Y. C.; Zielinski, D. C.; Haiman, Z. B.; Desouki, A. A.; Lercher, M. J.; Palsson, B. O. Machine Learning Applied to Enzyme Turnover Numbers Reveals Protein Structural Correlates and Improves Metabolic Models. *Nat. Commun.* **2018**, *9, 5252*.

(22) Ekins, S.; Puhl, A. C.; Zorn, K. M.; Lane, T. R.; Russo, D. P.; Klein, J. J.; Hickey, A. J.; Clark, A. M. Exploiting Machine Learning for End-To-End Drug Discovery and Development. *Nat. Mater.* **2019**, *18*, 435-441.

(23) Lin, X.; Duan, X.; Jacobs, C.; Ullmann, J.; Chan, C. Y.; Chen, S.; Cheng, S. H.; Zhao, W. N.; Poduri, A.; Wang, X.; Haggarty, S. J.; Shi, P. High-Throughput Brain Activity Mapping and Machine Learning as a Foundation for Systems Neuropharmacology. *Nat. Commun.* **2018,** *9*, 5142.

(24) Lussier, F.; Missirlis, D.; Spatz, J. P.; Masson, J. F. Machine-Learning-Driven Surface-Enhanced Raman Scattering Optophysiology Reveals Multiplexed Metabolite Gradients near Cells. *ACS Nano* **2019**, *13*, 1403-1411.

(25) Frey, N. C.; Wang, J.; Vega Bellido, G. I.; Anasori, B.; Gogotsi, Y.; Shenoy, V. B. Prediction of Synthesis of 2D Metal Carbides and Nitrides (MXenes) and Their Precursors with Positive and Unlabeled Machine Learning. *ACS Nano* **2019**, *13*, 3031-3041.

(26) Kim, E.; Huang, K.; Saunders, A.; McCallum, A.; Ceder, G.; Olivetti, E. Materials Synthesis Insights from Scientific Literature *via* Text Extraction and Machine Learning. *Chem. Mater.* **2017**, *29*, 9436-9444.

(27) Kim, E.; Huang, K.; Tomala, A.; Matthews, S.; Strubell, E.; Saunders, A.; McCallum, A.; Olivetti, E. Data Descriptor: Machine-Learned and Codified Synthesis Parameters of Oxide Materials. *Sci. Data* **2017**, *4*, 170127.

(28) Li, Z.; Xu, Q.; Sun, Q.; Hou, Z.; Yin, W.-J. Thermodynamic Stability Landscape of Halide Double Perovskites *via* High-Throughput Computing and Machine Learning. *Adv. Funct. Mater.* **2019**, *29*, 1807280.

(29) Masood, H.; Toe, C. Y.; Teoh, W. Y.; Sethu, V.; Amal, R. Machine Learning for Accelerated Discovery of Solar Photocatalysts. *ACS Catal.* **2019**, *9*, 11774-11787.

(30) Tran, K.; Ulissi, Z. W. Active Learning Across Intermetallics to Guide Discovery of Electrocatalysts for CO_2 Reduction and H_2 Evolution. *Nat. Catal.* **2018**, *1*, 696-703.

(31) Tang, B.; Lu, Y.; Zhou, J.; Wang, H.; Golani, P.; Xu, M.; Xu, Q.; Guan, C.; Liu, Z. Machine Learning-Guided Synthesis of Advanced Inorganic Materials. *Mater. Today*, **2020**, DOI: 10.1016/ j.mattod.2020.06.010.

(32) Zhang, B.; Liu, Y.; Ren, M.; Li, W.; Zhang, X.; Vajtai, R.; Ajayan, P. M.; Tour, J. M.; Wang, L. Sustainable Synthesis of Bright Green Fluorescent Nitrogen-Doped Carbon Quantum Dots from Alkali Lignin. *ChemSusChem.* **2019**, *12*, 4202-4210.

(33) Rizzo, C.; Arcudi, F.; Dordevic, L.; Dintcheva, N. T.; Noto, R.; D'Anna, F.; Prato, M. Nitrogen-Doped Carbon Nanodots-Lonogels: Preparation, Characterization, and Radical Scavenging Activity. *ACS Nano* **2018**, *12*, 1296-1305.

(34) Tao, S.; Lu, S.; Geng, Y.; Zhu, S.; Redfern, S. A. T.; Song, Y.; Feng, T.; Xu, W.; Yang, B. Design of Metal-Free Polymer Carbon Dots: A New Class of Room-Temperature Phosphorescent Materials. *Angew. Chem. Int. Ed.* **2018**, *57*, 2393-2398.

(35) Vallan, L.; Urriolabeitia, E. P.; Ruiperez, F.; Matxain, J. M.; Canton-Vitoria, R.; Tagmatarchis, N.; Benito, A. M.; Maser, W. K. Supramolecular-Enhanced Charge Transfer within Entangled Polyamide Chains as the Origin of the Universal Blue Fluorescence of Polymer Carbon Dots. *J. Am. Chem. Soc.* **2018**, *140*, 12862-12869.

(36) Li, W.; Li, M.; Liu, Y.; Pan, D.; Li, Z.; Wang, L.; Wu, M. Three Minute Ultrarapid Microwave-Assisted Synthesis of Bright Fluorescent Graphene Quantum Dots for Live Cell Staining and White LEDs. *ACS Appl. Nano Mater.* **2018**, *1*, 1623-1630.

(37) Han, Y.; Li, M.; Lai, J.; Li, W.; Liu, Y.; Yin, L.; Yang, L.; Xue, X.; Vajtai, R.; Ajayan, P. M.; Wang, L. Rational Design of Oxygen-Enriched Carbon Dots with Efficient Room-Temperature Phosphorescent Properties and High-Tech Security Protection Application. *ACS Sustainable Chem. Eng.* **2019**, *7*, 19918-19924.

(38) Wang, L.; Li, M.; Li, W.; Han, Y.; Liu, Y.; Li, Z.; Zhang, B.; Pan, D. Rationally Designed Efficient Dual-Mode Colorimetric/Fluorescence Sensor Based on Carbon Dots for Detection of pH and Cu^{2+} Ions. *ACS Sustainable Chem. Eng.* **2018**, *6*, 12668-12674.

(39) Wang, L.; Li, W.; Li, M.; Su, Q.; Li, Z.; Pan, D.; Wu, M. Ultrastable Amine, Sulfo Cofunctionalized Graphene Quantum Dots with High Two-Photon Fluorescence for Cellular Imaging. *ACS Sustainable Chem. Eng.* **2018**, *6*, 4711-4716.

(40) Jiang, L.; Ding, H.; Lu, S.; Geng, T.; Xiao, G.; Zou, B.; Bi, H. Photoactivated Fluorescence Enhancement in F,N-Doped Carbon Dots with Piezochromic Behavior. *Angew. Chem. Int. Ed.* **2019**, *58*, 1-7.

(41) Wang, J.; Hao, J.; Liu, D.; Qin, S.; Chen, C.; Yang, C.; Liu, Y.; Yang, T.; Fan, Y.; Chen, Y.; Lei, W. Flower Stamen-Like Porous Boron Carbon Nitride Nanoscrolls for Water Cleaning. *Nanoscale* **2017**, *9*, 9787-9791.

(42) Jiang, K.; Wang, Y.; Cai, C.; Lin, H. Conversion of Carbon Dots from Fluorescence to Ultralong Room-Temperature Phosphorescence by Heating for Security Applications. *Adv. Mater.* **2018**, *30*, e1800783.

(43) Jiang, K.; Wang, Y.; Gao, X.; Cai, C.; Lin, H. Facile, Quick, and Gram-Scale Synthesis of Ultralong-Lifetime Room-Temperature-Phosphorescent Carbon Dots by Microwave Irradiation. *Angew. Chem. Int. Ed.* **2018**, *57*, 6216-6220.

(44) Li, Q.; Zhou, M.; Yang, Q.; Wu, Q.; Shi, J.; Gong, A.; Yang, M. Efficient Room-Temperature Phosphorescence from Nitrogen-Doped Carbon Dots in Composite Matrices. *Chem. Mater.* **2016**, *28*, 8221-8227.

(45) Das, R.; Parveen, S.; Bora, A.; Giri, P. K. Origin of High Photoluminescence Yield and High SERS Sensitivity of Nitrogen-Doped Graphene Quantum Dots. *Carbon* **2020**, *160*, 273-286.

(46) Zhao, F.; Zhang, T.; Liu, Q.; Lü, C. Aphen-Derived N-Doped White-Emitting Carbon Dots with Room Temperature Phosphorescence for Versatile Applications. *Sens. Actuators, B* **2020**, *304*, 127344.

(47) Guo, H.; Wen, S.; Li, W.; Li, M.; Wang, L.; Chang, Q.; Zhang, J.; Lai, J.; Vajtai, R.; Ajayan, P. M.; Wu, M. A Universal Strategy to Separate Hydrophilic Hybrid-Light Carbon Quantum Dots Using Pure Water as Eluent. *Appl. Mater. Today* **2020,** *18*, 100528.

(48) Suryawanshi, S. B.; Mahajan, P. G.; Bodake, A. J.; Kolekar, G. B.; Patil, S. R. Carbazole Based Nanoprobe for Selective Recognition of Fe^{3+} Ion in Aqueous Medium: Spectroscopic Insight. *Spectrochim. Acta. A* **2017**, *183*, 232-238.

(49) Naik, V.; Zantye, P.; Gunjal, D.; Gore, A.; Anbhule, P.; Kowshik, M.; Bhosale, S. V.; Kolekar, G. Nitrogen-Doped Carbon Dots *via* Hydrothermal Synthesis: Naked Eye Fluorescent Sensor for Dopamine and Used for Multicolor Cell Imaging. *ACS Appl. Bio Mater.* **2019**, *2*, 2069-2077.
(50) Naik, V. M.; Gunjal, D. B.; Gore, A. H.; Pawar, S. P.; Mahanwar, S. T.; Anbhule, P. V.; Kolekar, G. B. Quick and Low Cost Synthesis of Sulphur Doped Carbon Dots by Simple Acidic Carbonization of Sucrose for the Detection of Fe^{3+} Ions in Highly Acidic Environment. *Diam. Relat. Mater.* **2018**, *88*, 262-268.
(51) Qi, H.; Teng, M.; Liu, M.; Liu, S.; Li, J.; Yu, H.; Teng, C.; Huang, Z.; Liu, H.; Shao, Q.; Umar, A.; Ding, T.; Gao, Q.; Guo, Z. Biomass-Derived Nitrogen-Doped Carbon Quantum Dots: Highly Selective Fluorescent Probe for Detecting Fe^{3+} Ions and Tetracyclines. *J. Colloid Interface Sci.* **2019**, *539*, 332-341.
(52) Li, Y.; Ren, J.; Sun, R.; Wang, X. Fluorescent Lignin Carbon Dots for Reversible Responses to High-Valence Metal Ions and Its Bioapplications. *J. Biomed. Nanotechnol.* **2018**, *14*, 1543-1555.

For Table of Contents Only.

Highly fluorescent CDs are fabricated by a machine learning-assisted synthesis approach for iron ion sensing.